Journal of Russian Laser Research, Volume 34, Number 3, May, 2013

INTENSITY DISTRIBUTION OF A CAPILLARY-DISCHARGE 46.9 nm SOFT X-RAY LASER

Yongpeng Zhao,[1] Han Wu,[1]* Yao Xie,[2] Shan Jiang,[1] Huaiyu Cui,[1] and Qi Wang[1]

[1] *Harbin Institute of Technology*
National Key Laboratory of Tunable Lasers
Harbin, 150080 P. R. China

[2] *Chinese Academy of Sciences, Changchun Institute of Optics and Fine Mechanics*
State Key Laboratory of Applied Optics
Changchun, 130033 P. R. China

*Corresponding author e-mail: schmeichel1992@126.com

Abstract

We realize a Ne-like Ar 46.9 nm soft X-ray laser pumped by a capillary discharge. The study of the laser-pulse-intensity distribution is important for applications of soft X-ray lasers. The intensity distribution demonstrates the gain distribution, plasma radius, and axial plasma density that contribute to the study of the laser-pulse formation. To measure the intensity in different positions of the X-ray laser spot, we moved transversally an X-ray diode (XRD) assembled with a slit. We obtain the one-dimensional intensity distribution. We find a laser divergence (FWHM) of 4.0 mrad. According to the gain-guided model, we calculate the intensity distribution. The measured divergence of 4.0 mrad roughly corresponds to a plasma radius a approximately equal to 230–250 μm and on-axis electron density $n_e \approx 8.0 \cdot 10^{18} - 9.0 \cdot 10^{18}$ cm^{-3}. The results of calculations indicate that the divergence of the intensity distribution increases when the plasma radius decreases and the on-axis electron density increases.

Keywords: capillary discharge, intensity distribution, slit scanning, gain-guided model.

1. Introduction

Soft X-ray lasers are used in the diagnostics of high-density plasma, material ablation, soft X-ray microscopy, and micromachining. In 1994, Rocca et al. first demonstrated a Ne-like Ar 46.9 nm soft X-ray laser pumped by a capillary discharge [1]. As for the intensity distribution, they obtained the time-resolved end-on soft X-ray images utilizing an X-ray pinhole camera [2]. With the MCP intensified CCD and the phosphor-screen assisted CCD, they measured the intensity distribution and divergence of different soft X-ray lasers [3, 4]. They adopted the gain-guided model to calculate the distribution and analyzed the key impacts theoretically [5]. In 1998, they performed systematic measurements of two-dimensional near-field and far-field intensity distributions of the laser and numerical modeling of the divergence and output beam pattern [6].

Tomassetti et al. reported the 46.9 nm soft X-ray laser output in 2002 [7]. In their experiments, an aluminum foil was used to cut the visible and ultraviolet radiation, and a slit (3 mm) was positioned in

Manuscript submitted by the authors in English on December 29, 2012.

front of the XRD characterizing the divergence to be 4 mrad. Slit scanning is practical to achieve the one-dimensional intensity distribution, but there was no theoretical simulation of the slit-scanning results in [7]. In 2004, the laser with a 0.6 mrad near-Gaussian central peak and a 5 mrad angular pedestal was constructed in [8], where the gain-guided model was used to explain the distribution dominated by a flat plateau of the electron density distribution, which leads to a low refraction at the center of the plasma column [9].

The results of the two groups show that the pinched plasma varies with the discharge conditions, and different plasma characteristics lead to different intensity distributions. Therefore, it is important to study the intensity distribution of the experimental apparatus. The intensity distribution under the experimental conditions of small current and low pressure has been rarely observed so far; in addition, the slit scanning method lacks a theoretical simulation model. We measure experimentally the intensity distribution at small currents and low pressure employing the slit scanning method. Using the gain-guided model, we calculate the intensity distribution and its divergence for the slit-scanning geometry. We calculate the on-axis electron density and the plasma radius corresponding to the experimental results. The intensity distribution reflects the parameters of the plasma and the laser-pulse formation. Therefore, our results may contribute to improving the laser pulse and increasing the applications of soft X-ray lasers.

2. Experimental Setup

The capillary-discharge device is described thoroughly in [10]. Figure 1 is a schematic of the experimental apparatus. The ceramic (Al_2O_3) capillary is 35 cm in length and 3 mm in diameter. The slit scanning method for measuring the intensity distribution is adopted from [7]. The slit is 0.9 mm wide. The XRD is positioned 74 cm from the capillary end. The intensity distribution is measured by shifting the XRD assembled with the slit.

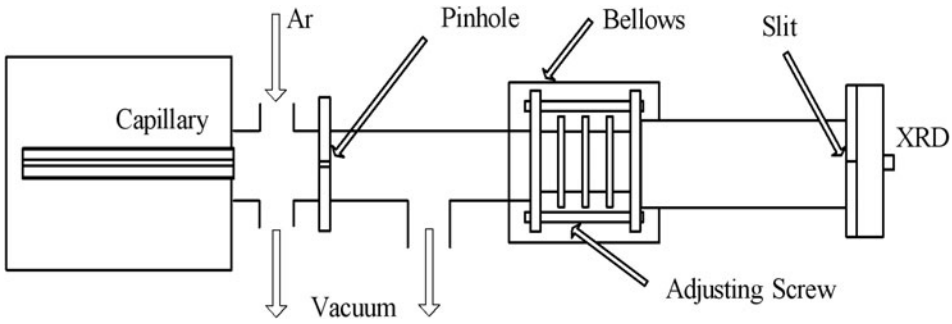

Fig. 1. Schematic of the experimental apparatus.

In order to guarantee the stability of the pressure and high vacuum of the XRD, a 1 mm diameter pinhole is positioned 1 cm from the capillary end. The beam diameter at the pinhole is comparable to the minimum plasma compressing radius 200–300 μm. Consequently, the pinhole is available for spatial filtering of the background emission and does not obstruct the laser beam.

The XRD and vacuum pipeline are connected with the bellows and adjusting screw, which enables the XRD to be moved along the horizontal direction. It is considered that the displacement of translational movement (typically a few millimeters) is much smaller than the detection distance. In order to observe the XRD displacement, a He–Ne laser is utilized as a mark on the XRD.

3. Experimental Results

The XRD is assembled with slit scans on the laser spot in order to record the intensity of the laser signal corresponding to different positions. Then we fit the experimental points of the laser signal with respect to the displacement to obtain the intensity distribution measured by slit scanning.

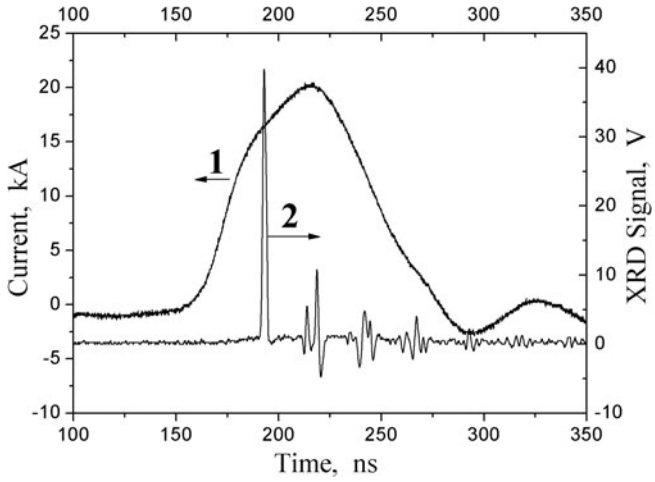

Fig. 2. The current pulse 1 and the XRD signal 2 with the slit at the spot center.

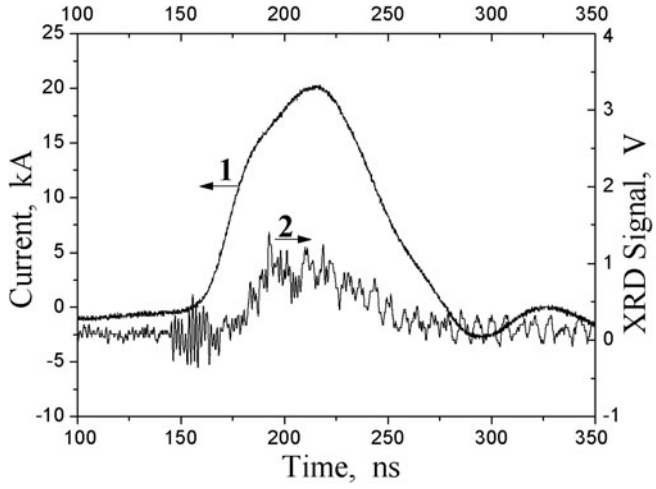

Fig. 3. The current pulse 1 and the XRD signal 2 with the slit at the fringe.

Figure 2 shows the current pulse and the XRD signal when the slit is located in the spot center. The peak belongs to the 46.9 nm laser owning to its high value and short duration of 1.6 ns. Figure 2 shows that the current peak is 20.4 kA and the rise time is 36.1 ns. Figure 3 shows the current pulse and the XRD signal when a 3 mm slit is located off-axis. The laser peak merges in the background, which means that the slit is located at the edge of the laser spot.

The discrete points in Fig. 4 represent the peak values of the XRD signal at different positions. Assuming that the intensity distribution profile is Gaussian [5], we show the fitting curve of the experimental points in Fig. 4. The divergence (FWHM) of the laser beam is 4.0 mrad. Unlike the signal of the X-ray CCD [9], the slit collects the intensity along a chord of the spot plane that we consider in our theoretical model.

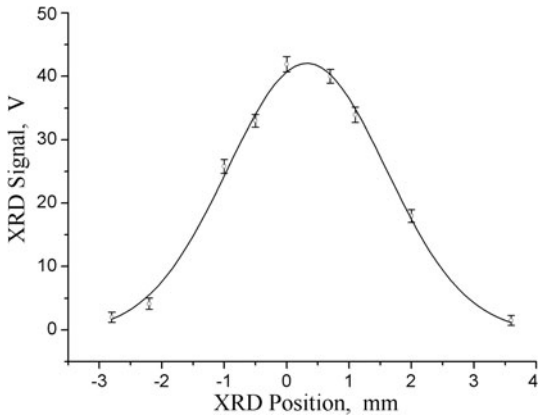

Fig. 4. Slit scanning results and the fitting curve.

4. Intensity-Distribution Model of Slit Scanning

The Z-pinch generated by a capillary discharge produces a high-temperature and high-density plasma. When the electron density reaches $3 \cdot 10^{18} - 1 \cdot 10^{19}$ cm^{-3} and the electron temperature reaches 60–80 eV [11], the Ne-like Ar ions are pumped from 3 s to 3 ps by the collision excitation. The 46.9 nm soft

X-ray laser pulse is formed.

The laser characteristics are determined by the plasma state. We derive a theoretical model from the gain-guided model [5]. The basic concept of the model assumes a steady state of the minimum compressed plasma when the laser pulse emits. The ray trajectory is determined by the ray-propagation equation, where the refractive index is described by a parabolic profile of the electron density. The intensity of a particular ray depends on the integrated gain length with respect to its propagation. Finally, we integrate the intensity of rays over the emitting plane and obtain the beam pattern.

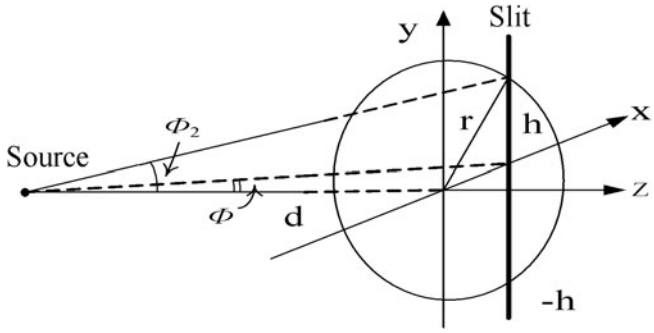

Fig. 5. Schematic of the theoretical model for calculating the slit incident intensity.

Figure 5 is a schematic of the theoretical model for calculating the slit incident intensity. The system of coordinates used is the same as in [5]. The z axis is coaxial with the cylinder, and the receiving surface is located on the x–y plane. The slit is perpendicular to the x axis where the line joining the pedal to the light source meets the z axis at an angle Φ. The angle Φ_2 is the angle between the line from a point on the receiving plane to the light source and the z axis, i.e.,

$$d^2 \tan^2 \Phi + h^2 = d^2 \tan^2 \Phi_2, \qquad \Phi_2 = \arctan\left(\pm\sqrt{\tan^2 \Phi + h^2/d^2}\right), \tag{1}$$

where d is the distance between the capillary end and the receiving plane, and h is the distance from a point on the plane to the x axis. The approximate formulas for the angular distribution of the fluxes of the on-axis and off-axis components are [5]

$$\begin{aligned} F_1(\Phi_2) &= \frac{8Sa^2\pi}{g_0 L_r} \exp\left[(g_0 - 2/L_r)l - g_0 L_r(\Phi_2/\Phi_r)^2/2\right], \\ F_2(\Phi_2) &= \sqrt{\frac{8\pi}{g_0 L_r}} \frac{Sa^2}{g_0 L_r - 1} \exp\left[(g_0 - 1/L_r)l - (g_0 L_r/2) - (\Phi_2 - \Phi_r)^2/2\sigma^2\right], \\ \sigma &= \frac{4\Phi_r^2}{g_0 L_r} \exp(-2l/L_r), \end{aligned} \tag{2}$$

where F_1 is the on-axis output flux, F_2 is the off-axis output flux, S is the source function computed, a is the minimum compressed plasma radius, g_0 is the on-axis maximum gain, and l is the capillary length. Define $L_r = a(n_c/n_e)^{1/2}$ and $\Phi_r = (n_e/n_c)^{1/2}$ as the characteristic values of the refraction length and angle, with n_c the critical density at the X-ray laser wavelength λ and n_e the on-axis electron density. The parabolic profile is used as an approximation to the electron density and gain distribution.

We substitute the expression of Φ_2 from Eqs. (1) to Eqs. (2) and integrate the flux over h in a reasonable range. Then the angular distribution of the intensity through the slit reads

$$I(\Phi) = \frac{\int \left[F_1(\Phi_2) + F_2(\Phi_2)\right] dh}{A\int dh} = \frac{\int \left[F_1(\Phi, h) + F_2(\Phi, h)\right] dh}{A\int dh}, \tag{3}$$

where $I(\Phi)$ is the intensity corresponding to Φ, and A is the spot area. Because the expressions for F_1 and F_2 are complicated, and analytic solutions do not exist, we resort to numerical calculations.

In Eq. (2), except the on-axis electron density n_e and the plasma radius a, the other variables can be obtained from the experiments and calculations. During laser operation, $n_e \sim 3 \cdot 10^{18} - 1 \cdot 10^{19}$ cm^{-3} and $a = 200 - 300$ μm [2]. Taking advantage of the derived geometric relation, we obtain the intensity distribution at different n_e and a.

5. Results of Calculations of the Intensity Distribution

We calculated numerically the intensity distribution of slit scanning using Eq. (2). Substituting a series of on-axis electron densities n_e and the plasma radius a within the discussed range, we obtain different distributions and divergences (FWHM).

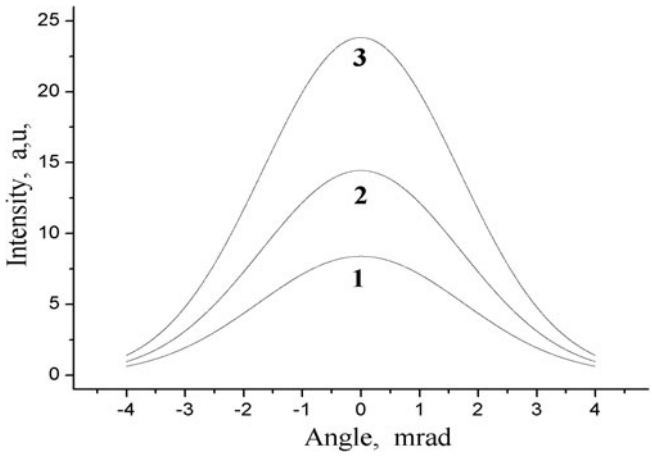

Fig. 6. Intensity distribution at $n_e = 8.5 \cdot 10^{18}$ cm^{-3} and $a = 230$ (curve 1), 240 (curve 2), and 250 μm (curve 3).

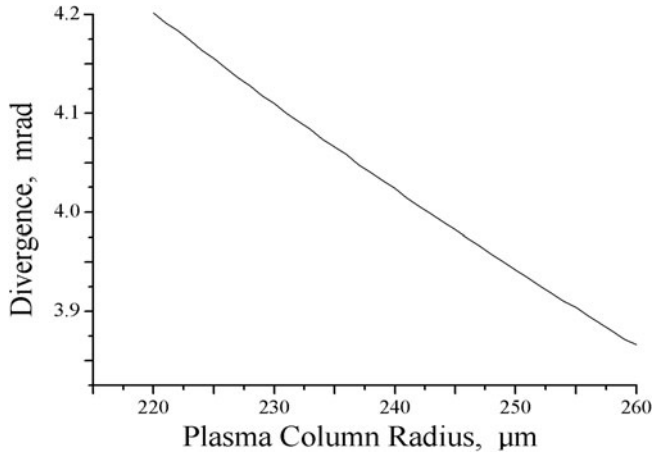

Fig. 7. Divergences as a function of the plasma radius at $n_e = 8.5 \cdot 10^{18}$ cm^{-3}.

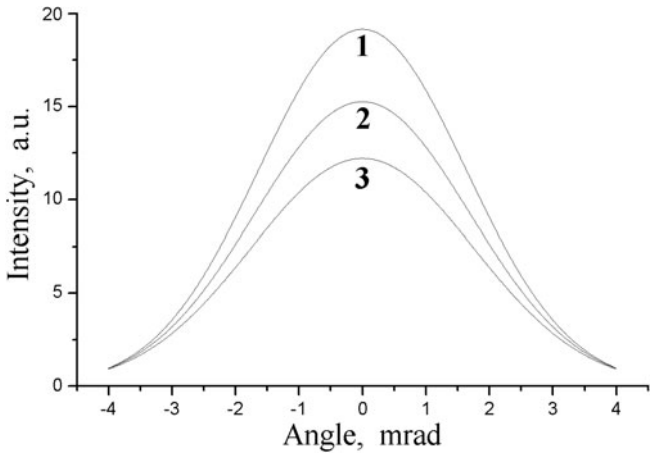

Fig. 8. Intensity distribution at $a = 240$ μm and $n_e = 8.0 \cdot 10^{18}$cm^{-3} (curve 1), $8.5 \cdot 10^{18}$ cm^{-3} (curve 2), and $9.0 \cdot 10^{18}$ cm^{-3} (curve 3).

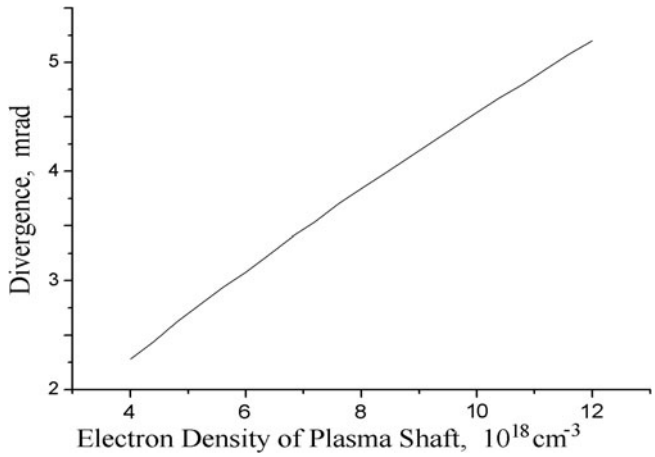

Fig. 9. Divergences as a function of the on-axis electron density at $a = 240$ μm.

We calculated the intensity distributions corresponding to different plasma radii. These distributions are shown in Fig. 6 at the on-axis electron density $n_e = 8.5 \cdot 10^{18}$ cm^{-3} and typical plasma radii $a = 230$, 240, and 250 μm. From Fig. 6, we see that the intensity amplitude increases with increase in the radius. The computed divergence (FWHM) with respect to the plasma radius is shown in Fig. 7. At ∼4.0 mrad, the radius changes from 220 to 260 μm and decreases approximately linearly.

The plasma electron density also influences the intensity distribution. With the plasma radius $a = 240$ μm, we calculated the intensity distributions with respect to the on-axis electron density. Figure 8 shows these distributions at $n_e = 8.0 \cdot 10^{18}$, $8.5 \cdot 10^{18}$, and $9.0 \cdot 10^{18}$ cm^{-3}. The intensity amplitude increases while the density decreases. It can be seen from Fig. 9 that the divergence (FWHM) increases approximately linearly as a function of the on-axis electron density. At 4.0 mrad, the electron density changes from $6.0 \cdot 10^{18}$ to $1.0 \cdot 10^{19}$ cm^{-3}.

In order to estimate the plasma radius and the on-axis electron density in our experiments, we performed a rough calculation, as shown in Fig. 10. According to the data obtained, we believe that the experimental intensity distribution with a divergence (FWHM) of 4.0 mrad corresponds to a ≈230–250 μm and $n_e \approx 8.0 \cdot 10^{18}$–$9.0 \cdot 10^{18}$ cm^{-3}. Even though this result is only an approximation, it, nevertheless, agrees with the experimental results, i.e., the calculation method is proved to be feasible.

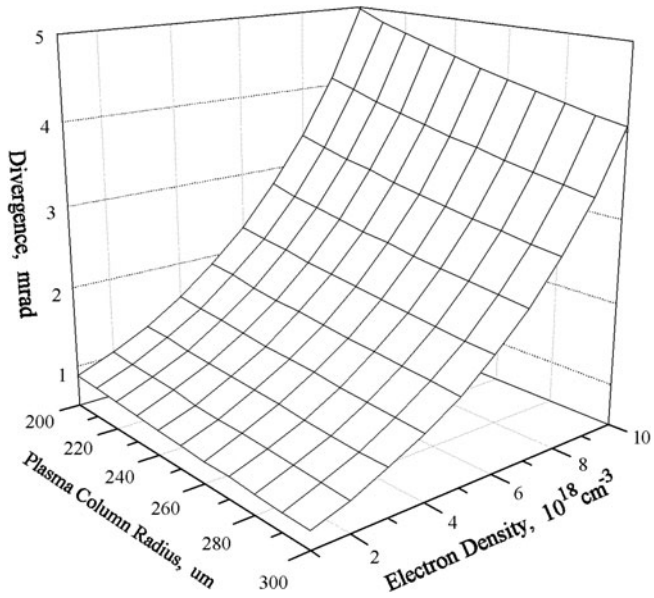

Fig. 10. Divergences as a function of the plasma radius and the electron density.

6. Conclusions

We reported on a slit scanning method for measuring the one-dimensional intensity distribution and a divergence (FWHM) of 4.0 mrad of a capillary-discharge Ne-like Ar 46.9 nm laser. We established a calculation model for the experimental results obtained. Within the reported range of the on-axis electron density and plasma radii, we obtained the distribution and divergence. The results of calculations indicate that the divergence increases when the plasma radius decreases and the on-axis electron density increases. The measured divergence (FWHM) of 4.0 mrad roughly corresponds to $a \approx 230$–250 μm and $n_e \approx 8.0 \cdot 10^{18} - 9.0 \cdot 10^{18}$ cm^{-3}. The experiment performed and the theory of the intensity distribution elaborated contribute to estimating the plasma parameters when the laser pulse is formed and can help to improve the laser pulse for different applications.

Acknowledgments

This study was supported by the National Natural Science Foundation of China under Project No. 61078034. We acknowledge the contributions of Prof. Yang Dawei from the China Atomic Energy Academy of Sciences.

References

1. J. J. Rocca, V. Shlyaptsev, F. G. Tomasel, et al., *Phys. Rev. Lett.*, **73**, 2192 (1994).
2. J. J. Rocca, F. G. Tomasel, M. C. Marconi, et al., *Phys. Plasmas*, **2**, 2547 (1995).
3. B. R. Benware, C. H. Moreno, D. J. Burd, and J. J. Rocca, *Opt. Lett*, **22**, 796 (1997).
4. B. R. Benware, C. D. Macchietto, C. H. Moreno, and J. J. Rocca, *Phys. Rev. Lett.*, **81**, 5804 (1998).
5. Juan L. A. Chilla and J. J. Rocca, *J. Opt. Soc. Am. B*, **13**, 2841 (1996).
6. C. H. Moreno, M. C. Marconi, V. N. Shlyaptsev, et al., *Phys. Rev. A*, **58**, 1509 (1998).
7. G. Tomassetti, A. Ritucci, A. Reale, et al., *Eur. Phys. J. D*, **19**, 73 (2002).
8. A. Ritucci, G. Tomassetti, A. Reale, et al., *Phys. Rev. A*, **70**, 023818 (2004).
9. A. Ritucci, G. Tomassetti, A. Reale, et al., *J. Appl. Phys. B*, DOI: 10.1007/s00340-004-1442-5 (2004).
10. Y. Zhao, Y. Cheng, B. Luan, et al., *J. Phys. D: Appl. Phys.*, **39**, 342 (2006).
11. J. J. Rocca, D. P. Clark, J. L. A. Chilla, and V. N. Shlyaptsev, *Phys. Rev. Lett.*, **77**, 1476 (1996).